1 Development of an in vitro platform for nutrient absorption studies as an alternative to in vivo pig models 2 3 Bo Ram Lee<sup>1,2,\*</sup>, Sun Keun Jung<sup>1</sup>, Sun A Ock<sup>1</sup>, Poongyeon Lee<sup>1</sup>, Jin Young Jeong<sup>3</sup>, Jae Gyu Yoo<sup>1</sup> 4 5 <sup>1</sup>Animal Biotechnology and Genomics Division, National Institute of Animal Science, Rural Development 6 Administration, Wanju 55365, Republic of Korea 7 <sup>2</sup>Department of Bio-medical Analysis, Bio Campus of Korea Polytechnics, Nonsan 32943, Republic of Korea 8 <sup>3</sup>Precision Animal Nutrition Division, National Institute of Animal Science, Rural Development Administration, 9 Wanju 55365, Republic of Korea 10 11 Running Title: In vitro model for nutrient absorption in pigs 12 13 \*Correspondence: Animal Biotechnology and Genomics Division, National Institute of Animal Science, Rural Development Administration, Wanju 55365, Republic of Korea. Tel.: +82 63 238 7259; Fax: +82 63 238 7297; E-14 15 mail: mirjujang@gmail.com 16 17 **Author Information** 18 Bo Ram Lee: mirjujang@gmail.com 19 Sun Keun Jung: raphi0930@gmail.com 20 Sun A Ock: ocksa@korea.kr 21 Poongyeon Lee: pylee@korea.kr 22 Jin Young Jung: jeong73@korea.kr 23 Jae Gyu Yoo: vetjack@korea.kr

#### Abstract

24

25

26

27

28

29

30

31

32

33

34

35

36

37

38

39

40

41

Intestinal organoids have emerged as powerful in vitro tools for modelling gut physiology. The intestinal epithelium, comprising a single layer of cells, plays a crucial role in nutrient absorption. However, threedimensional (3D) intestinal organoid have inherent structural limitations that restrict direct access to the apical surface and hinder precise functional assays. To address these challenges, this study aimed to establish twodimensional (2D) porcine intestinal organoids and develop a Transwell-based in vitro platform for assessing nutrient absorption. In this study, we successfully derived and characterized intestinal organoids from adult porcine ileal tissues, demonstrating genetic and physiological similarities to the native intestinal epithelium. Optimisation of the culture medium using L-WRN-conditioned medium supplemented with these two key molecules enabled efficient organoid maintenance and proliferation. Furthermore, 2D intestinal organoids exhibiting consistent intestinal stem cell (e.g. LGR5 and Bmi1) and epithelial marker (e.g. E-cadherin, Cytokeratin19) expression were established. Functional assays confirmed the uptake of glucose, amino acids, and fatty acids, thus replicating the functionality observed in the native small intestine. Taken together, our findings demonstrate that 2D porcine intestinal organoids closely mimic in vivo intestinal functionality and tissue architecture and provide an accessible and reproducible platform for nutrient absorption studies. The development of a Transwell-based culture system further enhances experimental precision, offering a viable alternative to in vivo models for studying intestinal physiology and improving pig productivity. Thus, this platform holds significant promise for practical applications in nutritional research.

42

Keywords: Porcine, Intestinal organoids, 2D Culture System, Transwell Platform, Nutrient absorption

44

45

46

47

48

49

50

51

43

#### Introduction

Pigs are an important source of protein, accounting for approximately 35% of global meat production [1]. One of the key factors in improving pig productivity is enhancing feed efficiency, which is closely associated with the maintenance of a healthy intestinal epithelium [2]. A healthy intestinal epithelium enhances nutrient absorption and provides protection against pathogenic infections, thereby contributing to overall improvements in pig productivity [3, 4, 5, 6]. The epithelial lining, comprising a single layer of specialised cells, serves as a critical interface for nutrient transport and as a protective barrier against pathogens and toxins [7, 8]. In porcine intestinal

research, IPEC-J2 cell line and *in vivo* animal experiments remain the primary models. However, IPEC-J2 cells consist of a single cell type and lack the structural complexity and cellular diversity of native intestinal tissue, limiting their physiological relevance in nutrient absorption and barrier function studies [7]. While animal experiments offer the physiological relevance, they are associated with ethical concerns, high costs and limited suitability for high-throughput analysis [9, 10], Therefore, developing a more physiological relevant and scalable *in vitro* platform such as intestinal organids, is essential to overcome these limitations.

In recent years, intestinal organoids (IOs) have offered remarkable potential for modelling homeostasis and disease, emerging as powerful tools for studying gut physiology *in vitro* [11]. Derived from adult stem cells, these organoids enable the expansion and preservation of primary epithelial cells, including enterocytes, goblet cells, and Paneth cells, and maintain a state closely resembling that of the native intestinal environment [12]. Therefore, IOs cultured in three-dimensional (3D) systems have gained significant attention as potential alternatives to *in vivo* models for studying various functions of the intestinal epithelium. Their cellular diversity enables them to closely mimic native tissue, offering new possibilities and opportunities for *in vitro* testing [13, 14, 15, 16]. To suppot this, L-WRN cell-derived conditioned medium (CM) effectively recreates the intestinal stem cell (ISC) niche by providing essential factors, facilitating robust IO culture [17]. However, despite their advantages, structural limitations remain, particularly for studying processes such as host-pathogen interactions and nutrient absorption, as organoids cultured in Matrigel exhibit an inward-facing (basal-out) structure [18, 19].

To address these challenges, two-dimensional (2D) culture systems have been introduced as an accessible platform for investigating epithelial function and maintaining the key characteristics of intestinal epithelial cells while providing unrestricted access to both the apical and basolateral surfaces [20, 21]. Furthermore, Transwell-based systems have been developed to enable the precise control of nutrient transport, permeability assays, and disease modelling, thereby replicating the dynamic intestinal microenvironment [22].

In this study, we aimed to establish and characterise 3D porcine ileum IOs derived from adult intestinal crypts and optimise the culture medium using L-WRN-CM supplemented with small molecules to enhance growth, stem cell maintenance, and differentiation. We subsequently developed 2D intestinal epithelial monolayers to overcome structural limitations and improve accessibility to the epithelial surface. We also implemented a Transwell-based *in vitro* platform to precisely analyse nutrient absorption and epithelial barrier function under controlled experimental conditions.

#### **Materials and Methods**

#### Experimental designs, animals, and animal care

- This study aimed to establish 3D and 2D IOs as well as an *in vitro* platform for nutrient absorption studies. For
- this purpose, ileal tissues from 10-month-old adult pigs (n=3) were used.

84

85

80

81

#### Isolation of intestinal crypts, including ISCs, and 3D culture

- 86 Porcine intestinal crypts were isolated from the ileal tissue of 10-month-old pigs following established protocols
- 87 [16]. After longitudinal cutting and thorough washing with a buffer containing 1% penicillin/streptomycin, the
- 88 tissues were incubated in a cell dissociation solution for 40 min at room temperature. Next, the crypts were
- dislodged by pipetting and collected by centrifugation at  $200 \times g$  for 5 min. The crypt pellet was then mixed with
- Matrigel at a 1:1 ratio (140–150 crypts per dome), plated in 24-well plates, polymerised at 37°C, and overlaid
- 91 with intestinal human organoid medium (Stem Cell Technologies, Vancouver, BC, Canada). Cultures were
- 92 incubated at 37°C with 5% CO<sub>2</sub> to support organoid formation.

93

94

#### Passaging of porcine IOs

- Porcine IOs were passaged weekly after maturation, as previously described [16]. The medium was aspirated, and
- 96 the wells were rinsed with ice-cold phosphate-buffered saline (PBS) without disturbing the Matrigel dome. For
- 97 harvesting, 1 mL of enzyme-free cell dissociation buffer was added per 100 μL of Matrigel, followed by 10 min
- of incubation at 37°C. Thereafter, organoids were dislodged by pipetting and collected by centrifugation at  $300 \times$
- 99 g for 5 min. The pellet was resuspended in a 1:1 mixture of culture medium and Matrigel, and 140-150
- organoids/well were redistributed into three wells of a 24-well plate.

101

102

#### Histology and immunohistochemistry of small intestine

- Small intestinal segments were washed with ice-cold PBS and fixed in 10% neutral-buffered formalin (Sigma-
- Aldrich, St. Louis, MO, USA). The tissues were embedded in paraffin, sectioned vertically and horizontally (3–
- 105 5-μm thick), de-paraffinised in xylene, rehydrated using an ethanol series, and stained with haematoxylin and
- eosin (H&E) (Merck, Darmstadt, Germany) to visualise the crypt-villus architecture and tissue integrity under a
- light microscope. For immunohistochemistry (IHC), sections were permeabilised with 0.1% Triton X-100,
- 108 blocked with 0.1% normal goat serum, and subjected to antigen retrieval using sodium citrate buffer. Samples

were incubated overnight at 4°C with primary antibodies, as shown in Table 1, followed by Alexa Fluor-488 and Alexa Fluor-594-conjugated secondary antibodies (Molecular Probes, Eugene, OR, USA). Nuclei were counterstained with diamidino-2-phenylindole (DAPI), and confocal images were captured using a Nikon AX microscope equipped with a 20x and 40x objective lens (Nikon Instruments Inc., Tokyo, Japan).

#### Immunofluorescence staining of porcine IOs

Organoids were cultured in 24-well plates until maturation. After removing the culture medium, organoids were washed with cold PBS and incubated in 4% paraformaldehyde (Sigma-Aldrich) for 30 min. Thereafter, cells were permeabilized with 0.5% Triton X-100 (Sigma-Aldrich) in PBS for 30 min. After blocking with 3% bovine serum albumin (BSA) in PBS for 1 h, the organoids were incubated overnight at 4°C with the appropriate primary antibodies (Table 1). Marker protein expression was detected using AlexaFluor-488 and AlexaFluor-594 secondary antibodies (Molecular Probes) for 1 h. Subsequently, the samples were counterstained with DAPI and mounted on slides with ProLong Gold Antifade (Life Technologies, Carlsbad, CA, USA).

#### Epithelial barrier permeability assay and fatty acid absorption

Epithelial barrier function was assessed using fluorescein isothiocyanate (FITC)-dextran (4 and 40 kDa; Sigma-Aldrich). Fully developed organoids with crypts and villous structures were cultured in 24-well plates. Each well was treated with 25 ng/mL FITC-dextran, and the plates were incubated under standard growth conditions. Luminal absorption of FITC-dextran was monitored, and fluorescence intensity was recorded at two time points (0 hr and 24 hr) using a Leica CTR6000 fluorescence microscope (Leica, Wetzler, Germany). For the fatty acid uptake assay, C1-BODIPY 500/510 C12 (Invitrogen, Carlsbad, CA, USA) was applied to the 2D IOs. The C1-BODIPY solution was prepared with fatty acid-free BSA at a 5 μM final concentration and incubated for 30 min. Fluorescent images were captured using a confocal microscope (Nikon Instruments Inc.).

#### L-WRN cell culture

L-WRN cells (CRL-3276; ATCC, Manassas, VA, USA) were maintained and passaged in Dulbecco's Modified Eagle Medium (DMEM; Invitrogen) supplemented with 10% foetal bovine serum (FBS) and 1× antibiotic—antimycotic solution at 37°C with 5% CO<sub>2</sub>. Cells containing plasmids for the expression of growth factors (mouse

Wnt3a, R-spondin 3 and Noggin) were selected over 3 days by adding 0.5 mg/mL G418 (Sigma-Aldrich) and 0.5 mg/mL Hygromycin B (Sigma-Aldrich) after seeding in T75 flasks. After the selection process, the cells were thoroughly washed with PBS to remove residual antibiotics and maintained in DMEM supplemented with 10% FBS and 1× antibiotic–antimycotic solution. The conditioned medium (L-WRN CM) was retrieved every day for 3 days and then pooled together by batch, along with the addition of two small-molecule compounds, 10 μM Y27632 (STEMCELL Technologies, Vancouver, BC, Canada) and 10 μM SB431542 (Sigma-Aldrich). Samples were kept at -20°C for long-term storage, and the expression levels of Wnt3a were quantified using Mouse Wnt-3a DuoSet ELISA (R&D Systems, Inc., Minneapolis, MN, USA) before use in the experiment. The viability of IOs cultured in L-WRN CM was determined using a Cell Counting Kit 8 (ab228554; Abcam, Cambridge, UK). The experiment was independently replicated thrice.

#### **RNA** isolation

Total RNA was isolated from the IOs and other prepared samples, such as the ileal tissues of 2- and 10-month-old pigs and muscle as a control, using TRIzol reagent (Life Technologies), following previously established protocols [23, 24]. RNA quality was evaluated using an Agilent 2100 Bioanalyzer equipped with an RNA 6000 Nano Chip (Agilent Technologies, Amstelveen, The Netherlands). RNA was quantified using a NanoDrop 2000 Spectrophotometer (Thermo Fisher Scientific, Waltham, MA, USA) to ensure high-quality RNA for downstream analyses.

#### Library preparation and sequencing

A QuantSeq 3' mRNA-Seq Sequencing A Library Prep Kit (Lexogen GmbH, Vienna, Austria) was used to construct libraries for both control and test RNAs, following the manufacturer's protocol. Briefly, 500 ng of total RNA was hybridised with an oligo-dT primer containing an Illumina-compatible sequence at its 5'-end, followed by reverse transcription. After the degradation of the RNA template, second-strand synthesis was performed using a random primer with an Illumina-compatible linker sequence at the 5'-end. The resulting double-stranded cDNA library was purified using magnetic beads to remove excess reaction components. The library was subjected to PCR amplification to integrate the adapter sequences necessary for cluster generation, followed by another purification step to remove the remaining PCR components. Finally, high-throughput single-end sequencing (75

bp) was performed using an Illumina NextSeq 500 platform (Illumina, San Diego, CA, USA). This efficient process produces high-quality sequencing libraries, enabling precise gene expression analysis and thorough bioinformatics processing.

168

169

170

171

172

173

174

175

176

177

178

179

180

181

182

183

184

185

165

166

167

#### Data analysis

QuantSeq 3' mRNA-Seq reads were aligned using Bowtie2 [25]. Alignment indices were generated from both the genome assembly and representative transcript sequences, allowing mapping to both the genome and transcriptome. The resulting alignment files were used for transcript assembly, abundance estimation, and differential gene expression analysis. Differentially expressed genes were identified based on read counts derived from both unique and multiple alignments, which were analysed using the coverage command in Bedtools [26]. The read count data were subjected to quantile normalisation using EdgeR within R (R Development Core Team, 2016; R Foundation for Statistical Computing, Vienna, Austria) and Bioconductor [27]. Statistical analyses of differential gene expression were performed by edgeR v3.40.2 [28] using raw counts as input. In the QC step, genes with non-zero counts in all replicates at least one period group were selected. PCA (Principal component analysis) and MDS (Multidimensional scaling) plot were generated to confirm the similarity of expression between samples. Filtered data set was applied with TMM Normalization to correct the variation of library sizes among samples. Statistical significance of differential expression gene was determined using edgeR exactTest. Fold change and p-value were extracted from the result of exactTest. All p-values are adjusted by Benjamini-Hochberg algorithm to control false discovery rate (FDR). Significant gene list was filtered by |fold change|≥2 and raw p-value < 0.05. QuantSeq 3' mRNA-Seq datasets are publicly available in the Gene Expression Omnibus (GEO) database under the accession codes GSE288735 and GSE288737.

186

187

188

189

190

191

192

193

## **Development of 2D IOs**

Porcine IOs were harvested from the Matrigel dome after 7 days of growth in ice-cold PBS, transferred to a 15-mL tube, and retrieved by centrifugation at  $300 \times g$  for 5 min. Thereafter, the pellets were incubated with TrypLE<sup>TM</sup> Express Enzyme (Thermo Fisher Scientific) for 10 min at 37°C. Organoids were then dissociated by gentle pipetting to obtain single-cell suspensions. Single cells were resuspended in intestinal human organoid medium (STEMCELL Technologies) and seeded at 78,000 cells/well in pre-coated 24 well plates or Transwells. The pre-coating procedure was performed through treatment with a 0.5% (v/v) Matrigel in DMEM/F12 medium

for 1 h at 37°C. Next, the coating solution was removed, and the wells were washed once with advanced DMEM/F12 medium before seeding the single cells. After 3 days of growth in intestinal human organoid medium (STEMCELL Technologies), the cell monolayers reached full confluence and were used for further experiments.

#### Transepithelial-transendothelial electrical resistance (TEER) analysis

After 7 days of growth, the porcine IOs were harvested from the Matrigel dome and dissociated into single cells. Transwell inserts in the apical chamber were coated with a 0.5% (v/v) Matrigel in DMEM/F12 medium for 1 h at 37°C. The prepared cells, including 2D IOs, were seeded onto 24-well Transwell inserts containing 0.33-μm pore size filters at a density of 78,000 cells/well. Bovine ear fibroblast (BEF) was used as a control. The TEER was measured using a voltmeter (World Precision Instruments, Sarasota, FL, USA) approximately 3-4 days after seeding.

#### qRT-PCR

Quantitative RT-PCR was performed to assess the expression of several ISC and the epithelial markers in porcine IOs at passage 10, with muscle tissue used as a control. Total RNA (1 μg) was reverse-transcribed using a Superscript III First-Strand Synthesis System (Invitrogen). The PCR reaction mixture was prepared by adding 2 μL PCR buffer, 1.6 μL 2.5 mM dNTP, 10 pmol each forward and reverse primer, 1 μL 20× Eva green, 0.2 μL Taq DNA polymerase, and 2 μL cDNA to a final volume of 20 μL. PCR was performed by means of an initial incubation at 94°C for 3 min, followed by 40 cycles at 94°C for 30 s, 60°C for 30 s, and 72°C for 30 s, using a melting curve program (increasing temperature from 55 to 95°C at a rate of 0.5°C per 10 s) and continuous fluorescence measurement. Sequence-specific products were identified using a melting curve. Gene expression was analysed using a StepOnePlus<sup>TM</sup> Real-Time PCR System (Applied Biosystems, Foster City, CA, USA) and calculated using the 2-ΔΔCt method [29]. The qPCR primers used for each target gene are summarised in Table 2.

## Amino acids, glucose, and fatty acid uptake assays

2D IOs were seeded at a density of  $1x10^4$  cells/well onto a 96-well microplate, and the cells were cultured at  $37^{\circ}$ C overnight in a 5% CO<sub>2</sub> incubator. Afterwards, the culture medium was removed, and the cells were washed with pre-warmed Hanks' balanced salt solution (HBSS). After incubation with pre-warmed HBSS at  $37^{\circ}$ C for 5 min, a

pre-warmed BPA uptake solution (Dojindo Molecular Technologies, Rockville, MD, USA) was added to the 2D IOs and incubated at 37°C for 5 min in a 5% CO<sub>2</sub>. Thereafter, the supernatant was removed, and a pre-warmed working solution was added and incubated at 37°C for 5 min. The fluorescence intensity was measured at 415 nm. For the glucose (ab136956; Abcam) and fatty acid (ab176768; Abcam) uptake assays, 2D IOs were seeded in a 96-well plate. The cells were starved by replacing the growth medium with serum-free, glucose-free medium and incubating them at 37°C for 2 h. Working solutions of the 2-NBDG fluorescent glucose (for glucose uptake) and fatty acid fluorescent (for fatty acid uptake) analogues were prepared according to the manufacturer's instructions and added to each well containing starved cells. The cells were then incubated at 37°C for 30 min to allow for the uptake of glucose and fatty acid analogues. After incubation, the cells were washed thoroughly with PBS, and the fluorescence intensity was measured using a microplate reader. The exciatation/emission wavelengths were set at 535/587 nm for glucose uptake and 485/515 nm fro fatty acid uptake, respectively.

#### Quantitation of glucose and amino acids using a Transwell culture system

Transwell inserts in the apical chamber were coated with 0.5% (v/v) Matrigel diluted in DMEM/F12 medium for 1 h at 37°C, after which the prepared 2D IOs were seeded onto the 24-well Transwell inserts. Following treatment with glucose and amino acids, the glucose and amino acid contents in both the apical and basolateral compartments were measured using an IDEXX Catalyst Dx Chemistry Analyser (IDEXX Laboratories, Inc., Westbrook, ME, USA) equipped with a Chem 17 Clip and an Agilent HPLC DAD/FLD detector with Pickering 1260 (Agilent Technologies, Santa Clara, USA), respectively.

#### Statistical analysis

- All data are presented as means ± standard error of the mean, derived from three independent experiments.
- 244 Significant differences between groups were determined using either one-way ANOVA or Student's t-test,
- depending on the experimental design. A P-value  $\leq 0.05$  was considered statistically significant (\* $P \leq 0.05$ ).

#### Results

#### **Derivation and culture of porcine IOs**

Intestinal crypts were isolated from the small intestine (ileum) of healthy pigs (10 months old), sequentially

embedded in Matrigel, and cultured in Intesticult medium. Figure 1A illustrates the experimental procedures for isolating intestinal crypts and the culture of ileum-derived IOs in pigs. To validate the epithelial integrity and intestinal crypt-villus architecture, H&E staining was histologically performed using the intestinal ileum tissues. Detailed examination of vertical sections from ileal tissues revealed an intact intestinal epithelium structure, characterised by crypts located at the base and finger-like villi extending towards the apical side, indicating the growth potential in intestinal organoid derivation (Figure 1B). As shown in Figure 1C, the organoids were long-term maintained over more than 10 passages, indicating stable growth. Additionally, IHC was performed to identify ISCs *in vivo* using several markers specific to intestinal stem and epithelial cells. As shown in Figure 1D and Additional Figure 1, intestinal crypts exhibited distinct expression patterns of ISC markers, such as leucine-rich repeat-containing G protein-coupled receptor 5 (*LGR5*) and B lymphoma Mo-MLV insertion region 1 homology (*Bmi1*). Furthermore, fluorescence staining revealed the epithelium-specific expression of E-cadherin and F-actin in adherent junctions and the intestinal epithelial cytoskeleton.

#### Gene expression profiling and cellular potentials of porcine IOs

To investigate the genetic properties of porcine IOs for large-scale gene expression profiling, we used QuantSeq 3' mRNA-Seq and constructed a library. The scatter plot in Figure 2A reveals that specific genes related to ISC markers, such as LGR5 and hepatocyte nuclear factor 4 alpha (HNF4A), and epithelium makers, such as E-cadherin (CDHI) for adherent junctions, Mucin2 (MUC2) for goblet cells, Chromogranin A (CHGA) for enteroendocrine cells, and GATA binding protein 6 (GATA6) for the differentiation and maturation of intestinal epithelial cells markers, were significantly upregulated in IOs at passage 5 (P5) compared with those in muscle as a negative control and the ileal tissues of 2- (2M-I) and 10-month-old (10M-I) pigs. Principal component analysis (PCA) and heat maps indicated that the distance between the IOs and small intestine was relatively close compared with that for muscle in pigs (Additional Figure 2). In addition, (PCR) results showed that intestinal epithelium, including (PCM) (PCM) and (PCM) (PCM)

Moreover, IOs at P5 were positive for a proliferating cell marker (Ki67) and showed epithelium-specific expression against E-cadherin for adherent junctions and cytokeratin 19 for enterocytes. Furthermore, we examined the paracellular permeability of the epithelial layer to assess epithelial barrier integrity, within 24 h of treatment using fluorescent tracers. FITC-dextran successfully labelled the organoid lumen, indicating high permeability to compounds up to 4 kDa. In contrast, FITC-dextran, with a molecular weight of 40 kDa, did not penetrate the organoid lumen (Figure 2D and Additional Figure 3).

284

285

286

287

288

289

290

291

292

293

294

295

296

297

298

299

300

301

302

303

304

305

278

279

280

281

282

283

#### **Development of L-WRN CM for culturing porcine IOs**

We previously reported the establishment of porcine IOs derived from the jejunal tissue of the small intestine of pigs [16]. In the present study, we established ileum-derived IOs and utilized L-WRN conditioned medium (CM) to reconstitute the intestinal stem cells niche of porcine ileum in vitro or to replace IntestiCult<sup>TM</sup> medium used for the 3D culture of IOs. L-WRN cells were genetically modified to secrete three critical factors, Wnt3a, R-spondin 3, and Noggin, which enable the mimicry of the ISC niche [30]. L-WRN cells grow as an adherent monolayer with an elongated and spindle-shaped morphology (Figure 3A). As shown in Figure 3B, the quantity of Wnt3a in L-WRN CM in each batch after drug treatment was measured. Furthermore, L-WRN CM culture medium was optimised by adding two small-molecule compounds, Y27632 and SB431542, enabling the efficient maintenance and proliferation of ileum-derived IOs (Figure 3C). The Pearson's coefficient of porcine ileum-derived IOs cultured using Intesticult medium (OGM) and L-WRN CM was 0.94, while that between OGM and medium comprising a 1:1 mixture of OGM and L-WRN CM (OGM + L-WRN CM) was 0.99, indicating high similarity in gene expression levels (Figure 3D and Additional Figure 4). However, the scatter plot revealed that specific genes related to epithelial markers, such as MUC2 for goblet cells and CHGA for enteroendocrine cells in porcine ileum-derived IOs, were significantly downregulated in L-WRN CM compared with those in conventional OGM. In contrast, OGM and medium comprising a 1:1 mixture of OGM and L-WRN CM did not differ, indicating that it can be used more effectively for IO in porcine (Figure 3E). Therefore, the data suggest that L-WRN CM alone may have functional limitations, combining it with OGM effectively support both proliferation and differentiation, providing a more balanced environment for growth. More Importantly, porcine ileum-derived IOs in L-WRN CM plus OGM were well maintained beyond P5 and exhibited a distinct branched morphology on Day 7 at each passage, with no significant difference in total number, supporting their stable differentiation potentials (Figure

3F and Additional Figure 5).

307

308

309

310

311

312

313

314

315

316

317

318

319

320

321

322

323

324

325

326

327

328

329

330

306

#### Development of an in vitro platform for nutrient absorption using 2D IOs

2D IOs were generated by disrupting IOs after 7 days of growth within the Matrigel dome using a single-cell suspension (Figure 4A). We investigated the spatial expression of several specific markers associated with ISC and epithelial characteristics to examine the cellular potential of the 2D IOs. As shown in Figure 4B, the expression of Bmi1, an ISC marker, and E-cadherin, Cytokeratin 19, and Mucin2, epithelial markers, was confirmed. This indicated that the concomitant expression of ISC and epithelial genes in 2D IOs is very similar to that in IOs derived from intestinal crypts and mimics the topology of an in vivo intact intestine. Notably, we observed that fully confluent 2D organoids transformed into intestinal-like structures through self-organisation when cultured continuously for 2 weeks. Furthermore, after 3 days of culture, the fully confluent 2D IOs reproducibly presented a TEER value, as a measure of tight-junction integrity, between 100 and 200  $\Omega$  cm<sup>2</sup> in Transwell inserts, while BEF, as a control, exhibit values within the range of 10 to 20 Ω·cm² (Figure 4C). The 2D IOs expressed intestinal adult stem cell and epithelial cell markers (Figure 4B). In addition, the activity of glucose (GLUT2) and peptide (PEPT1) transporters, as well as fatty acid uptake in the 2D IOs, was confirmed (Figure 4D). To further assess nutrient uptake in the 2D IOs, we confirmed the accurate measurement of nutrient uptake using fatty acids, amino acids, and glucose analogues. As shown in Figure 4E, the 2D IOs exhibited significant absorption capacity. A Transwell-based culture system using 2D IOs was developed to mimic nutrient absorption in vitro (Figure 5A). The cellular permeability of confluent 2D organoid monolayers was analysed using 40 kDa fluorescein-conjugated dextran and a fluorimeter in the Transwell system. We confirmed that the 40 kDa fluorescein-conjugated dextran showed no paracellular leakage under our conditions (Additional Figure 5). Each assay was performed using organoids derived from at least two independent donors and there technical replicates were conducted per donor. Specifically, we used this system to evaluate the absorption levels of glucose and essential amino acids and measured their quantities in the upper and lower compartments of the Transwell system after 24 h. The 2D IOs actively absorbed glucose and amino acids (Figure 5B and 5C).

331

332

333

#### Discussion

Our findings demonstrate that 2D porcine ileum-derived IOs cultured in Transwell inserts retain the

functional properties of the native small intestine and offer a reliable *in vitro* platform for nutrient absorption studies. This approach bridges the gap between conventional 3D IOs and *in vivo* models, paving the way for more precise nutrition and gut physiology research.

In this study, we successfully established 3D ileum-derived IOs from the ileal tissue of a 10-month-old pig. These organoids closely recapitulated the structure and cellular composition of the native small intestinal epithelium. Histological and immunohistochemical analyses confirmed the presence of villus-like structures with distinct expression of intestinal stem cells (ISCs) and epithelial markers in the source tissue (Figure 1). The maintenance of epithelial homeostasis in the small intestine relies on the continuous renewal of cells derived from ISCs residing in the villi [31, 32]. Our identification of LGR5<sup>+</sup> ISCs supports the regenerative capacity of the established IOs.

Previous studies have highlighted the pivotal role of ISCs in maintaining the self-renewing and differentiating capacity of intestinal organoids [12, 33, 34]. ISCs differentiate into various mature epithelial cell types, including absorptive enterocytes, mucus-secreting goblet cells, hormone-producing enteroendocrine cells, and antimicrobial peptide-producing Paneth cells [14, 15]. Our findings are consistent with earlier reports emphasizing that IOs can preserve the stem cell niche and sustain epithelial tissue integrity under *in vitro* conditions [34, 35]. Collectively, these results highlight the physiological relevance of ileum-derived IOs as a highly reproducible platform for studying porcine intestinal biology.

Gene expression profiling further supported the cellular diversity and genetic fidelity of the porcine IOs, revealing high similarity to native iteal tissue. In contrast to monolayer systems such as IPEC-J2 cells that comprise a single epithelial cell type, IOs encompass multiple specialized cell types, including ISCs, Paneth cells, enterocytes, and enteroendocrine cells [10, 15]. Upregulation of key genes, including ISC and epithelial markers, and the transcriptomic similarity to native tissue underscore the IOs' potential to retain *in vivo*-like genetic characteristics. Moreover, the expression of ISC markers (LGR5, Bmi1), epithelial markers (E-cadherin, cytokeratin 19), and the proliferation marker Ki67 further confirmed the presence of a heterogeneous cell population derived from adult stem cells.

Functional validation of IOs demonstrated their capacity for epithelial barrier integrity. Permeability assays revealed that 4 kDa FITC-dextran could penetrate the organoid lumen, whereas 40 kDa FITC-dextran was excluded (Figure 2), consistent with prior observations in porcine IOs [14, 36]. In contrast, chicken-derived IOs

did not permit entry of either FITC-dextran 4 kDa or 40 kDa in basal-out or apical-out configurations [6]. These findings further support the conclusion that porcine ileum-derived IOs closely mimic the functional characteristics of native intestinal epithelium. However, some limitations must be acknowledged. Structural heterogeneity among organoids and variability in epithelial tightness may restrict their ability to fully replicate *in vivo* nutrient absorption dynamics. In addition, differences in molecular permeability and potential leaky regions within the epithelial layer may impact experimental consistency. Further refinement of organoid architecture and standardization of culture conditions are needed to enhance their physiological accuracy and reproducibility in nutrient transport and toxicology studies.

Overall, this study demonstrates the feasibility and relevance of porcine ileum-derived IOs as a reliable *in vitro* model for intestinal research. By providing a multicellular, physiologically relevant platform, these IOs hold promise for applications in nutrient absorption studies, disease modeling, and the development of alternatives to animal experimentation.

Moreover, to reconstruct the ISCs niche *in vitro*, we developed an alternative culture system using L-WRN conditioned medium (CM) in place of the conventional IntestiCult medium. The optimized medium, supplemented with key niche factors including Wnt3a, R-spondin 3, and Noggin, along with the small molecules Y-27632 and SB-431542, successfully supported ISC maintenance and enhanced epithelial differentiation in ileum-derived IOs. Y-27632, a Rho-associated protein kinase (ROCK) inhibitor, is known to prevent cell apoptosis and help preserve the stem cell pool, while SB-431542 inhibits the TGF-β/BMP signaling pathway [12, 37].

Activation of high Wnt and low BMP signaling is critical for ISC maintenance and expansion, whereas low Wnt and high BMP signaling promote differentiation of intestinal epithelial cells [34, 38]. Compared to previous studies, our culture system utilized undiluted CM collected directly from L-WRN cells, which may have provided a consistent environment for ISC proliferation and organoid development. Notably, transcriptomic analyses confirmed the compatibility and adaptability of L-WRN CM in porcine IO culture. Interestingly, a slight reduction in epithelial marker expression was observed, which may reflect an enhanced potential for cellular differentiation in the established ileum-derived IOs. These findings suggest that the use of undiluted L-WRN CM, together with specific small molecules, effectively reconstructs the ISC niche and supports both stemness and differentiation capacity *in vitro* (Figure 3). This optimized culture strategy enhances the physiological relevance of porcine IOs and provides a flexible system for advanced studies in intestinal biology and epithelial homeostasis. Collectivley,

Our results clearly demonstrate that L-WRN CM plus OGM induced significant differentiation at each passage in porcine ileum-derived IOs, leading to the formation of complex, branched structures from initial spheroids.

To date, substantial efforts have been made to develop intestinal organoids (IOs) from various livestock species, including chicken [6, 39], pig [22, 40, 41], cattle [42, 43], dog [44], horse [45], and goat [46]. Although these organoid systems offer numerous opportunities for advancing intestinal research, their practical applications remain limited. In this context, we aimed to establish an *in vitro* platform for nutrient absorption studies by utilizing 2D porcine intestinal organoids cultured on Transwell inserts.

A major advantage of the 2D IO model is its accessibility to the apical surface, enabling rapid and reproducible formation of a confluent monolayer for studies of nutrient transport and epithelial permeability [47]. In the present study, we developed a versatile protocol for generating 2D porcine ileum-derived IOs from disrupted 3D structures. These monolayers specifically expressed the key markers associated with intestinal stem cells (Bmi1) and epithelial identity, including E-cadherin, cytokeratin 19, and mucin 2. Importantly, the transepithelial electrical resistance (TEER) values measured on Transwell inserts reflected tight junction integrity and were consistent with values previously reported for intact intestinal epithelium [48]. This suggests that 2D porcine ileum-derived IOs effectively replicate barrier functions that are essential for maintaining epithelial homeostasis and selective permeability, making them a reliable model for evaluating nutrient absorption [30]. In addition, the absence of FITC-dextran 40 kDa paracellular leakage further validated the integrity of the epithelial barrier, and transport dynamics were confirmed using fatty acids, amino acids, and glucose analogs (Figure 4). However, the detailed dose-dependent and time-course absorption experiments will be required in future studies to more precisely characterize the transport mechanisms in our 2D IO model. Collectively, these findings demonstrate that 2D IOs provide a physiologically relevant *in vitro* platform for investigating nutrient transport and intestinal barrier function under controlled conditions.

Finally, we applied the Transwell-based culture system using 2D porcine ileum-derived IOs to evaluate nutrient absorption under controlled conditions. Specifically, this system enabled precise quantification of glucose and essential amino acid uptake by measuring concentrations in the apical and basolateral compartments following 24-hour treatment, as daily feed intake is a critical parameter in standard pig feeding protocols. Our results confirmed that 2D IOs actively absorbed these nutrients, demonstrating functional similarity to the native intestinal epithelium. The formation of a uniform monolayer enhanced experimental reproducibility and allowed

for quantitative assessment (Figure 5). These findings underscore the importance of developing reliable *in vitro* platforms for nutrient absorption studies as alternatives to *in vivo* porcine models. Furthermore, the nutrient absorption assay helps determine the nutritional value of a diet more accurately than simply measuring the nutrient content of the feed by revealing how well a pig actually absorbs specific nutrients and nutritionists can formulate more efficient and cost-effective diets. Although this study focused on establishing a simplified epithelial monolayer for nutrient absorption assessment, we recognize that incorporating co-culture with stromal or immune cells could provide a more physiologically relevant *in vitro* model, particularly for evaluating host-microbe interaction, inflammation and barrier dysfunction.

In conclusion, this study successfully achieved two major objectives in the research of porcine small intestinal organoids. First, by optimizing the culture conditions, we established the L-WRN conditioned medium, which proved to be more efficient than the conventional commercial medium. This optimization enabled the reproduction of various epithelial cell types and physiological characteristics of the intestinal epithelium. The improved culture conditions contributed to the development of porcine small intestinal organoids as a reliable *in vitro* model.

Second, we developed a Transwell-based 2D organoid system that overcame the structural limitations of conventional 3D culture systems, enabling precise studies on nutrient absorption and intestinal barrier function. TEER measurements and FITC-dextran permeability assays confirmed strong barrier functionality, and the nutrient absorption kinetics closely resembled those of the native small intestine. These findings highlight the potential of the Transwell-based 2D organoid system as a valuable tool for future nutritional studies and disease modeling.

## **Competing Interests**

The authors declare that they have no competing interests.

#### Acknowledgements

We would like to sincerely thank TNT Research Co., Ltd. for helping large-scale gene expression data generation, analysis, GEO registration. This work was carried out with the support of "Cooperative Research Program for Agriculture Science and Technology Development (Project No. PJ01671901)" Rural Development Administration

446 (RDA), Republic of Korea. 447 448 **Authors' contributions** BRL participated in study design and coordination. BRL and SKJ carried out the experiments, statistical analysis. 449 450 BRL wrote manuscript. BRL, SKJ, SAO, PL, JYJ and JGR were involved in data interpretation. BRL and JGR 451 participated in writing the final versions of the manuscript. All authors have read and approved the final 452 manuscript. 453 454 Ethics approval and consent to participate 455 Ethical approval was granted by the Institutional Animal Care and Use Committee (IACUC) of the National 456 Institute of Animal Science, Korea (NIAS-2022-0569). All experimental procedures, including sample collection and handling, were conducted in accordance with the standard operating protocols of the Animal Biotechnology 457 458 Division of the National Institute of Animal Science, Korea.

## 460 Figure Legends

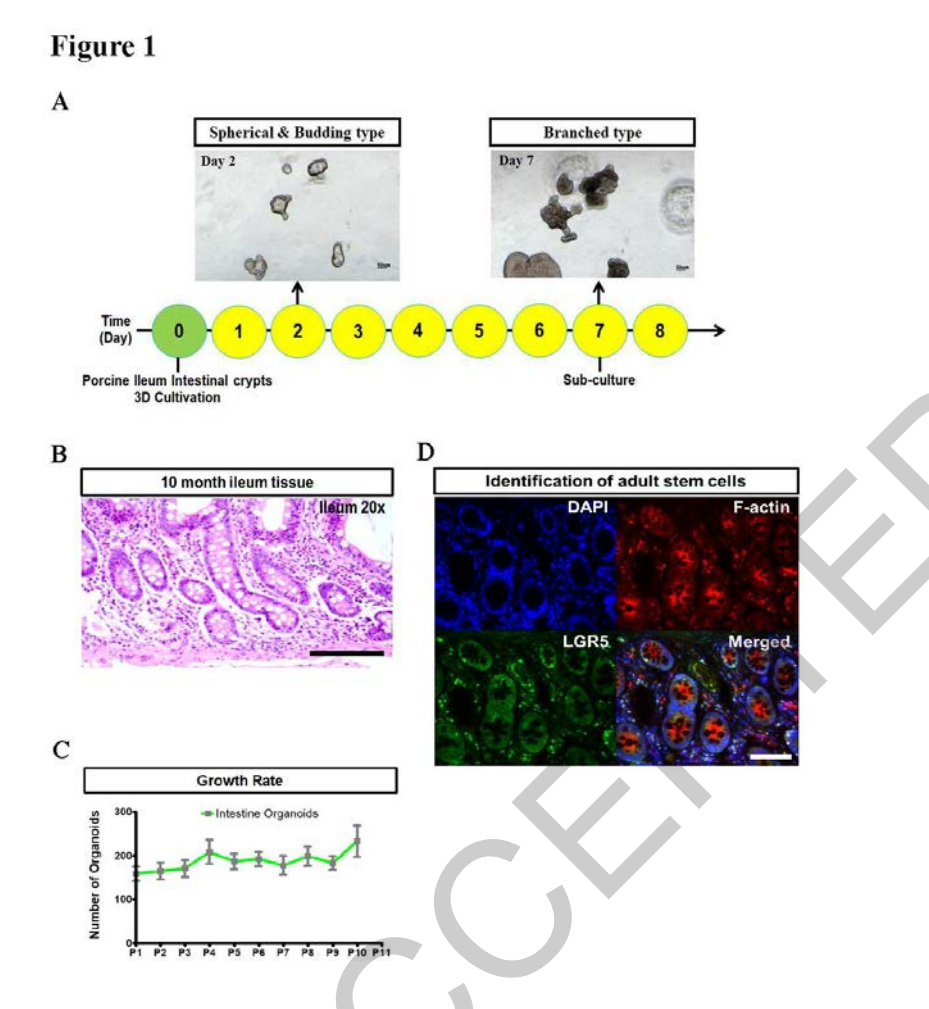


Figure 1. Growth performance in 3D culture of porcine ileum-derived intestinal organoids. (A) Porcine ileum-derived intestinal organoids grown in 3D culture showing spheroidal (round-shaped) morphology on day 2 and mature villi and crypt-like structures on day 7 at each passage. Spherical: 50 μm, Branched: 50 μm. (B) Haematoxylin and eosin staining to identify distinct crypt and villus structures from the ileal tissue of 10-monthold pigs. Scale bar: 20 μm. (C) Growth rate of porcine ileum-derived intestinal organoids presented as the number of organoids/well (mean n = 3 wells) growing in a 100-μL Matrigel dome in each well. Intestinal organoids were maintained for up to 10 generations without loss of the recapitulating capacity of crypts. (D) Immunohistochemistry of LGR5 and F-actin in the ileal tissue of the porcine small intestine. The fluorescently stained crypts were counterstained with diamidino-2-phenylindole. Scale bar: 20 μm

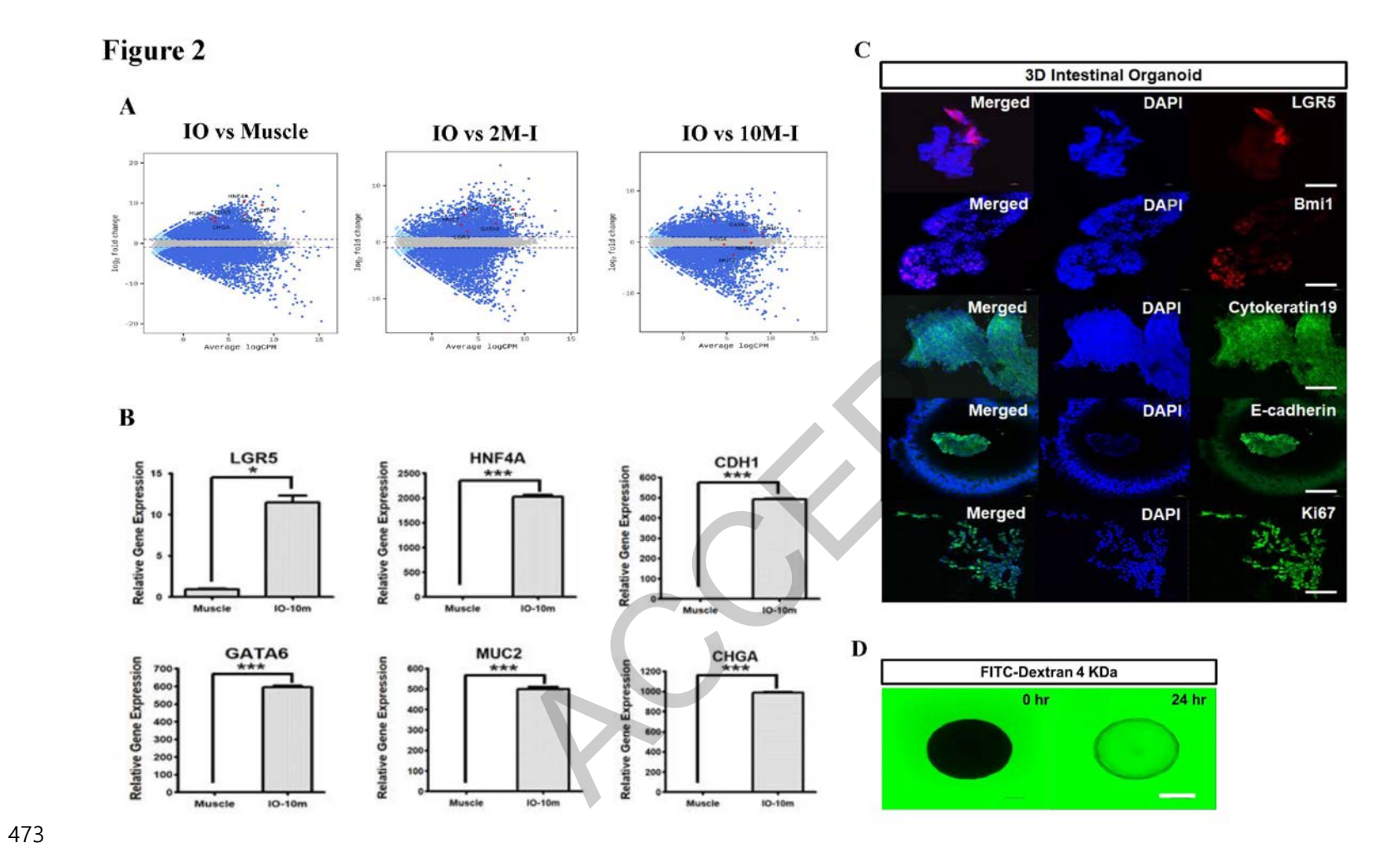


Figure 2. Characterisation and cellular potentials of porcine ileum-derived intestinal organoids. (A) Scatter plot showing the expression patterns of intestinal stem cell (*LGR5* and *HNF4A*) and epithelial (*CDH1* for adherent junctions, *MUC2* for goblet cells, *CHGA* for enteroendocrine cells and *GATA6* for the differentiation and maturation of intestinal epithelial cells markers, which were significantly upregulated in intestinal organoids (IOs) at passage 5 (P5) compared with those in muscle as a negative control. Porcine ileum-derived IOs at P5 were significantly upregulated or similar to the intestine. (B) Gene expression profiling of porcine ileum-derived IOs. qRT-PCR was performed to evaluate the gene expression of porcine ileum-derived IOs using several intestinal stem cell (*LGR5* and *HNF4A*) and epithelial (*CDH1*, *MUC2*, *CHGA* and *GATA6*) markers characteristics, with the muscle as a control. Gene expression was analysed using the 2-ΔΔCt method. Significant differences between groups were analysed using Student's *t*-test. A *p*-value less than or equal to 0.05 indicated statistical significance (\* $p \le 0.05$ , \*\*\* $p \le 0.001$ ). (C) Immunostaining of LGR5, Bmi1, Cytokeratin 19, E-cadherin and Ki67 in 3D porcine ileum-derived IOs at P5. The fluorescently stained organoids were counterstained with diamidino-2-phenylindole. Scale bar: 20 μm. (D) Paracellular permeability of the epithelial layer in porcine ileum-derived intestinal organoids using fluorescent tracers. Scale bar: 100 μm.

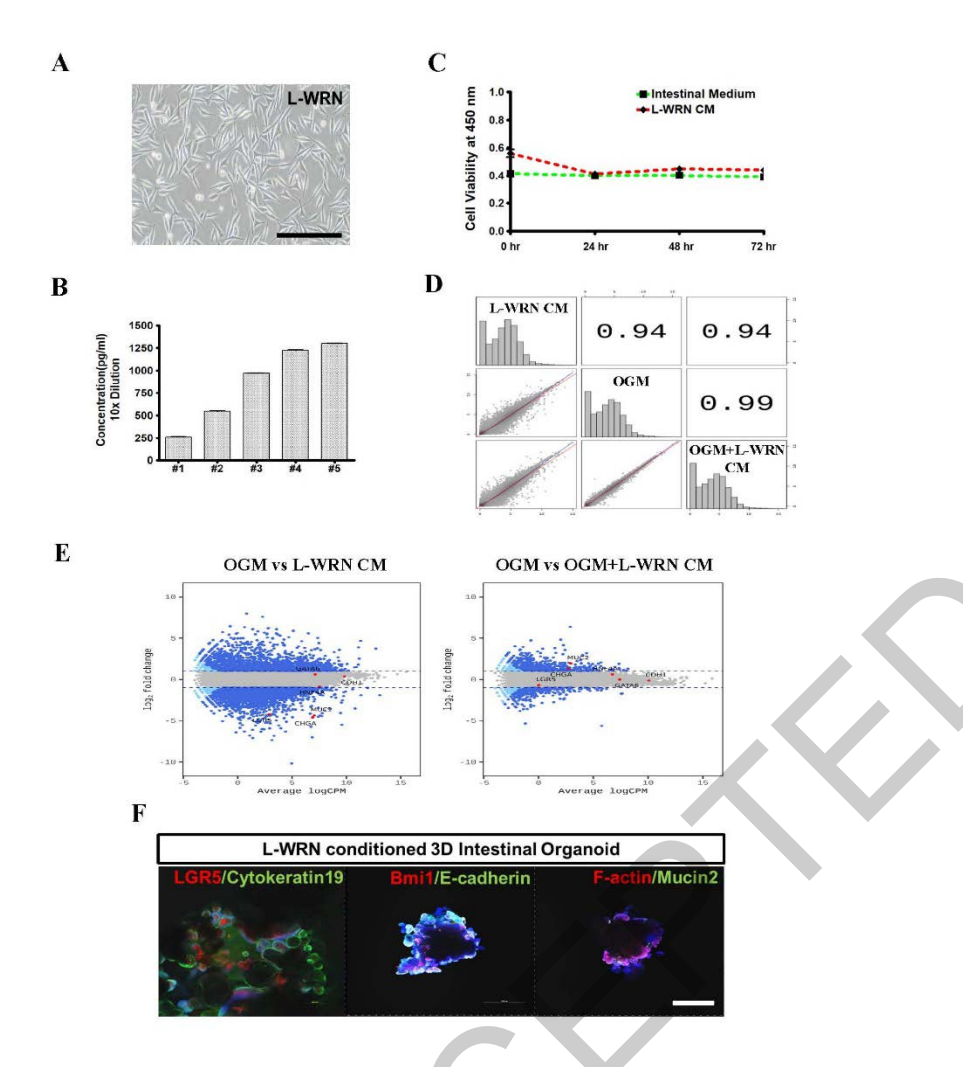


Figure 3. Development of L-WRN CM for culturing porcine intestinal organoids. (A) L-WRN cells grow as an adherent monolayer with an elongated and spindle-shaped morphology. Scale bar: 200 μm. (B) Identification and quantification of Wnt3a in L-WRN CM for each batch after drug treatment using Mouse Wnt-3a DuoSet ELISA. (C) Cell viability of intestinal organoids cultured in L-WRN CM was determined using a Cell Counting Kit 8. The experiment was independently replicated thrice. (D) Pearson's coefficient for porcine ileum-derived intestinal organoids cultured in Intesticult medium (OGM) and L-WRN CM, as well as in their combination (OGM + L-WRN CM). (E) Scatter plot revealing the upregulation of specific genes related to the epithelial markers of porcine ileum-derived intestinal organoids cultured in L-WRN CM and the comparison between OGM + L-WRN CM and OGM. (F) Immunostaining of LGR5, Bmi1, F-actin, E-cadherin, Cytokeratin 19, and MUC2 in porcine ileum-derived intestinal organoids cultured in L-WRN CM. The fluorescently stained organoids were counterstained with diamidino-2-phenylindole. Scale bar: 100 μm.

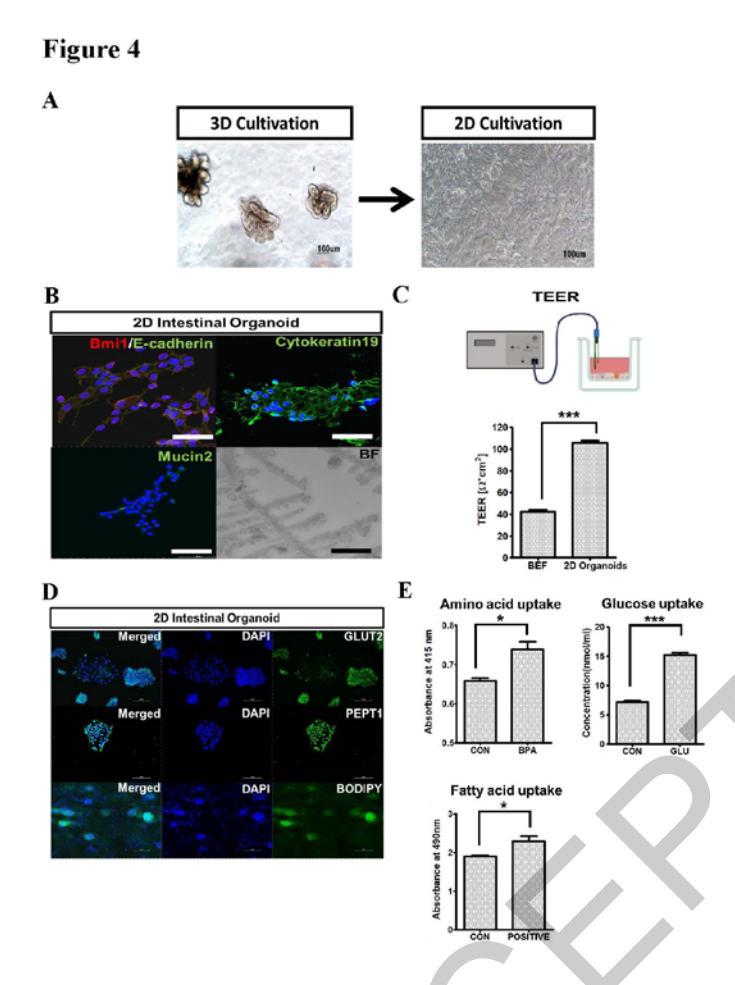
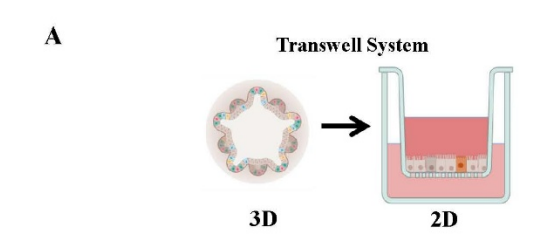
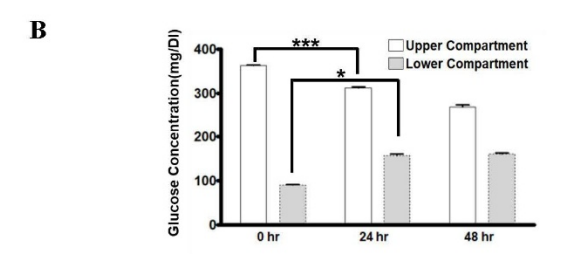


Figure 4. Generation and characterisation of 2D intestinal organoids. (A) 2D intestinal organoids were generated by disrupting 3D intestinal organoids after 7 days of growth within a Matrigel dome using a single-cell suspension. (B) Immunostaining of Bmi1, Cytokeratin 19, E-cadherin, and Mucin2 in 2D intestinal organoids. The organoids were counterstained with diamidino-2-phenylindole. Scale bar: 100 μm. (C) Transendothelial electrical resistance (TEER) value of fully confluent 2D intestinal organoids after 3 days of culture was measured with bovine ear fibroblast (BEF) as the control. (D) Glucose (GLUT2) and peptide (PEPT1) transporter activity and fatty acid uptake in 2D intestinal organoids. The fluorescent organoids were counterstained with diamidino-2-phenylindole. Scale bar: 100 μm. (E) Accurate measurement of nutrient uptake using fatty acids, amino acids, and glucose analogues in 2D intestinal organoids. The experiment was independently replicated thrice.







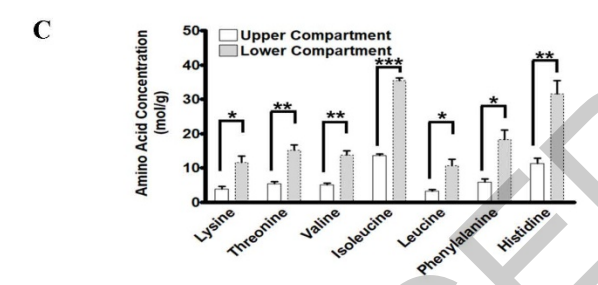
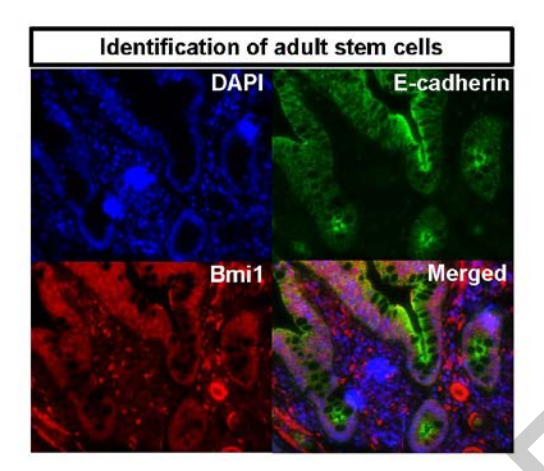


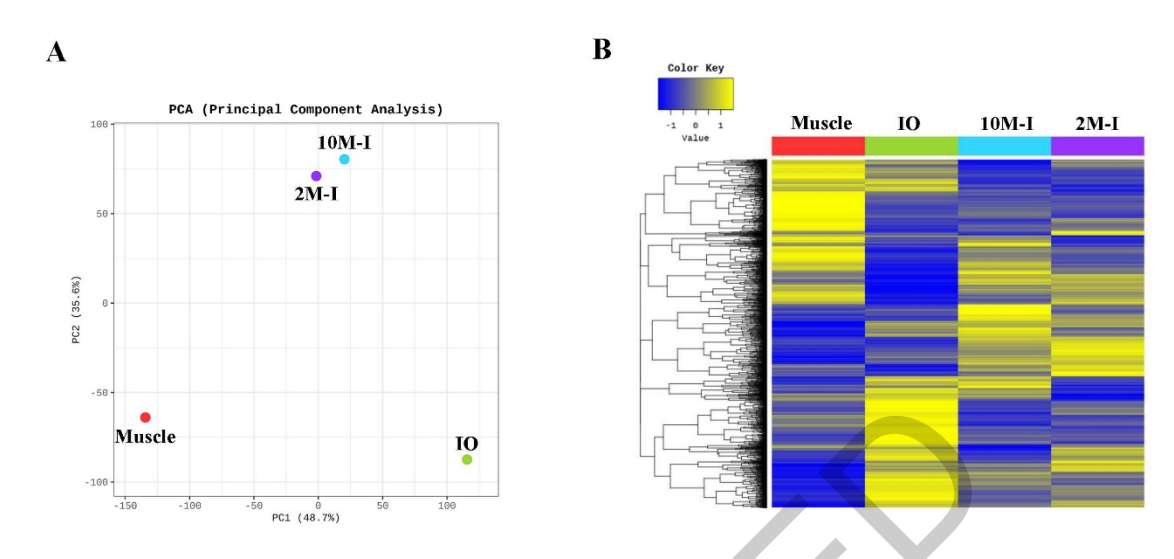
Figure 5. Development of an *in vitro* platform for precisely measuring nutrient absorption. (A) A Transwell-based culture system with 2D intestinal organoids for evaluating nutrient absorption under controlled conditions. (B) The glucose content in both the apical and basolateral compartments was measured using an IDEXX Catalyst Dx Chemistry Analyser equipped with a Chem 17 Clip after treatment with glucose. The experiment was independently replicated thrice. Significant differences between groups were determined using Student's *t*-test. A *p*-value less than or equal to 0.05 indicated statistical significance (\* $p \le 0.05$ , \*\*\* $p \le 0.001$ ). (C) The amino acid content in both the apical and basolateral compartments was measured using an Agilent HPLC DAD/FLD detector with a Pickering 1260 after treatment with amino acids. The experiment was independently replicated thrice. Significant differences between groups were determined using Student's *t*-test. A*p*-value less than or equal to 0.05 indicated statistical significance (\* $p \le 0.05$ , \*\* $p \le 0.01$ , \*\*\* $p \le 0.001$ ).

# **Additional Figure 1**



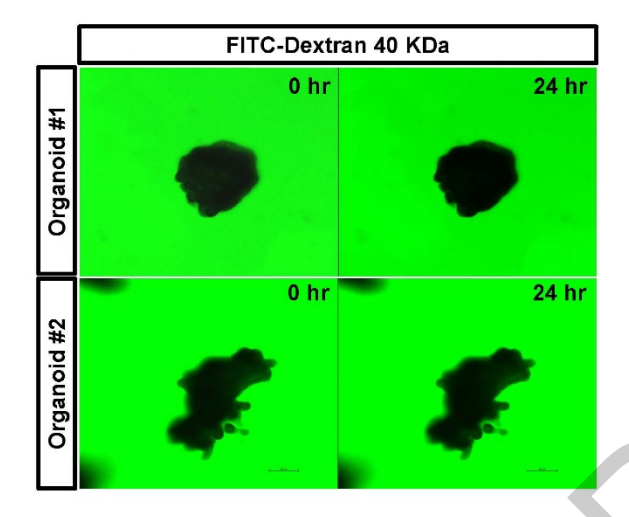
Additional Figure 1. Characterisation of porcine ileal tissue. Immunohistochemistry of Bmi1 and E-cadherin in porcine ileal tissue. Fluorescently stained crypts were counterstained with diamidino-2-phenylindole. Scale bar:  $20 \ \mu m$ .

# **Additional Figure 2**



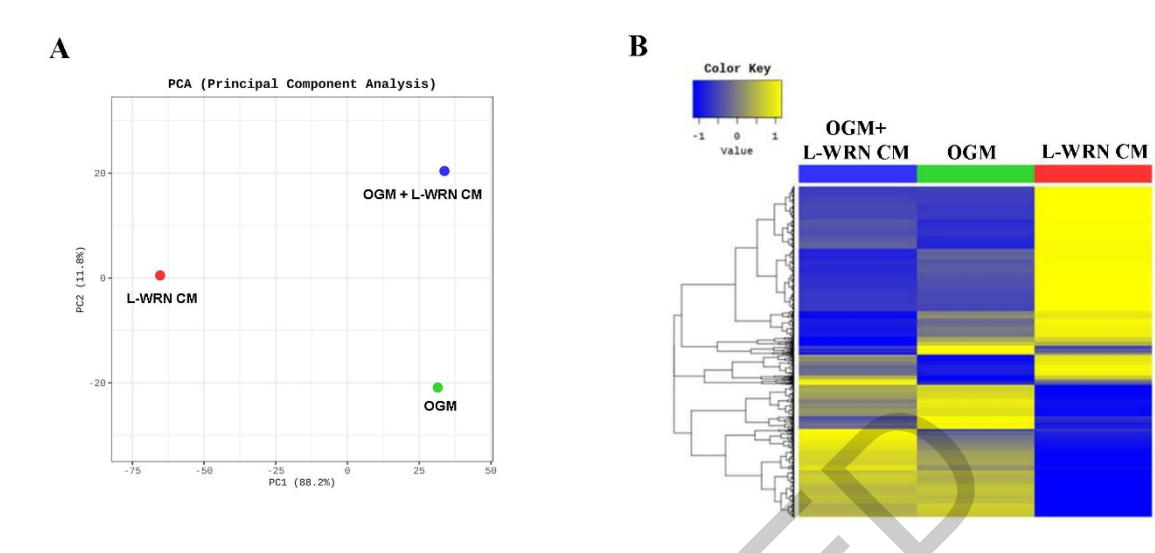
Additional Figure 2. Gene expression profiling of porcine ileum-derived intestinal organoids. (A) Principal component analysis (PCA) of intestinal organoids (IOs) at passage 5 (P5) compared with muscle and the ileal tissue of 2- (2M-I) and 10-month-old (10M-I) pigs. (B) Hierarchical clustering showing that several genes between the porcine ileum-derived IOs and 2M-I or 10M-I are shared and similarly expressed compared with those in the muscle (control).

# **Additional Figure 3**



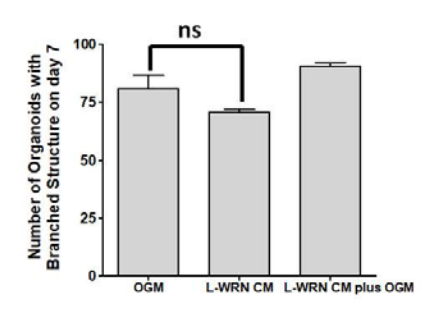
Additional Figure 3. Cellular potentials of porcine ileum-derived intestinal organoids. Paracellular permeability of the epithelial layer in porcine ileum-derived intestinal organoids using fluorescent tracers. Scale bar:  $100 \, \mu m$ .

# **Additional Figure 4**



Additional Figure 4. Gene expression profiling of porcine ileum-derived intestinal organoids cultures in L-WRN CM. (A) Principal component analysis (PCA) of porcine ileum-derived intestinal organoids cultured in Intesticult medium (OGM) and L-WRN CM, as well as in their combination (OGM + L-WRN CM). (B) Hierarchical clustering showing that several genes in ileum-derived intestinal organoids cultured in OGM and L-WRN CM and OGM + L-WRN CM are shared and similarly expressed.

# Additional Figure 5



**Additional Figure 5.** The number of porcine ileum-derived intestinal organoids with the branched structure cultured in Intesticult medium (OGM) and L-WRN CM, as well as in their combination (OGM + L-WRN CM) on Day 7. Significant differences between groups were analyzed by Student's t test. The difference between the groups is not statistically significant.

# **Additional Figure 6**

# Absorbance at 490 nm Upper FD 40 kDa Lower FD 40 kDa Negative

Additional Figure 6. Cellular potentials of porcine 2D intestinal organoids in a Transwell-based culture system. The cellular permeability of confluent 2D organoid monolayers was analysed in a Transwell system using a 40 kDa fluorescein-conjugated dextran and fluorimeter. The experiment was independently replicated thrice.

## References 1. Bruinsma J. World agriculture: towards 2015-2013, an FAO perspective. London: Food Agric Organ United Nations; 2003. p. 1-432. 2. Patience JF. Ed. Feed efficiency in swine. Wageningen Academic Publishers. 2012. 3. Ewing WN, Desmond JAC. The living gut: an introduction to micro-organisms in nutrition. 1994. 4. Willing BP, Malik G, Van Kessel AG. Nutrition and gut health in swine. Sustainable swine nutrition. 2013;197-213. 5. Inamul H, Hyeon Y, Sun AO, Ha-Yeon W, Kang-Won P, Poong-Yeon L, et al. Recent Progress and Future Perspectives on Intestinal Organoids in Livestock. Journal of Agriculture & Life Science. 2021;55(5):83-90. 6. Kang TH, Lee SI. Establishment of a chicken intestinal organoid culture system to assess deoxynivalenol-induced damage of the intestinal barrier function. J Anim Sci Biotechnol. 2024;15(1):30. 7. Brosnahan AJ, Brown DR. Porcine IPEC-J2 intestinal epithelial cells in microbiological investigations. Vet Microbiol. 2012;156(3-4):229-37. 8. Kang TH, Shin S, Park J, Lee BR, Lee SI. Pyroptosis-Mediated Damage Mechanism by Deoxynivalenol in Porcine Small Intestinal Epithelial Cells. Toxins (Basel). 2023;15(4). 9. Che L, Zhou Q, Liu Y, Hu L, Peng X, Wu C, et al. Flaxseed oil supplementation improves intestinal function and immunity, associated with altered intestinal microbiome and fatty acid profile in pigs with intrauterine

10. Hamilton CA, Young R, Jayaraman S, Sehgal A, Paxton E, Thomson S, et al. Development of in vitro enteroids

growth retardation. Food Funct. 2019;10(12):8149-60.

derived from bovine small intestinal crypts. Vet Res. 2018;49(1):54.
11. Rahmani S, Breyner NM, Su HM, Verdu EF, Didar TF. Intestinal organoids: A new paradigm for engineering
intestinal epithelium in vitro. Biomaterials. 2019;194:195-214.
12. Sato T, Vries RG, Snippert HJ, van de Wetering M, Barker N, Stange DE, et al. Single Lgr5 stem cells build
crypt-villus structures in vitro without a mesenchymal niche. Nature. 2009;459(7244):262-5.
13. Rallabandi HR, Yang H, Oh KB, Lee HC, Byun SJ, Lee BR. Evaluation of Intestinal Epithelial Barrier
Function in Inflammatory Bowel Diseases Using Murine Intestinal Organoids. Tissue Eng Regen Med.
2020;17(5):641-50.
14. Lee BR, Yang H, Lee SI, Haq I, Ock SA, Wi H, et al. Robust Three-Dimensional (3D) Expansion of Bovine
Intestinal Organoids: An In Vitro Model as a Potential Alternative to an In Vivo System. Animals (Basel).
2021;11(7).
15. Park KW, Yang H, Lee MG, Ock SA, Wi H, Lee P, et al. Establishment of intestinal organoids from small
intestine of growing cattle (12 months old). J Anim Sci Technol. 2022;64(6):1105-16.
16. Lee BR, Ock SA, Park MR, Lee MG, Byun SJ. Establishing porcine jejunum-derived intestinal organoids to
study the function of intestinal epithelium as an alternative for animal testing. Journal of Animal Reproduction
and Biotechnology. 2024;39(1):2-11.
17. Mussard E, Pouzet C, Helies V, Pascal G, Fourre S, Cherbuy C, et al. Culture of rabbit caecum organoids by
reconstituting the intestinal stem cell niche in vitro with pharmacological inhibitors or L-WRN conditioned
medium. Stem Cell Res. 2020;48:101980.
18. Takeda N, Jain R, LeBoeuf MR, Wang Q, Lu MM, Epstein JA. Interconversion between intestinal stem cell
populations in distinct niches. Science. 2011;334(6061):1420-4.

624	19. Wilson SS, Tocchi A, Holly MK, Parks WC, Smith JG. A small intestinal organoid model of non-invasive
625	enteric pathogen-epithelial cell interactions. Mucosal Immunol. 2015;8(2):352-61.
626	
627	20. van der Hee B, Loonen LMP, Taverne N, Taverne-Thiele JJ, Smidt H, Wells JM. Optimized procedures for
628	generating an enhanced, near physiological 2D culture system from porcine intestinal organoids. Stem Cell
629	Res. 2018;28:165-71.
630	
631	21. Tretola M, Bee G, Silacci P. Gallic acid affects intestinal-epithelial-cell integrity and selected amino-acid
632	uptake in porcine in vitro and ex vivo permeability models. Br J Nutr. 2021;126:492-500.
633	
634	22. Li Y, Yang N, Chen J, Huang X, Zhang N, Yang S, et al. Next-Generation Porcine Intestinal Organoids: an
635	Apical-Out Organoid Model for Swine Enteric Virus Infection and Immune Response Investigations. J Virol.
636	2020;94(21).
637	
638	23. Lee BR, Kim H, Park TS, Moon S, Cho S, Park T, et al. A set of stage-specific gene transcripts identified in
639	EK stage X and HH stage 3 chick embryos. BMC Dev Biol. 2007;7:60.
640	
641	24. Lee BR, Rengaraj D, Choi HJ, Han JY. A novel F-box domain containing cyclin F like gene is required for
642	maintaining the genome stability and survival of chicken primordial germ cells. FASEB J. 2020;34(1):1001-
643	17.
644	
645	25. Langmead B, Salzberg SL. Fast gapped-read alignment with Bowtie 2. Nat Methods. 2012;9(4):357-9.
646	
647	26. Quinlan AR, Hall IM. BEDTools: a flexible suite of utilities for comparing genomic features. Bioinformatics.
648	2010;26(6):841-2.
649	
650	27. Gentleman RC, Carey VJ, Bates DM, Bolstad B, Dettling M, Dudoit S, et al. Bioconductor: open software
651	development for computational biology and bioinformatics. Genome Biol. 2004:5(10):R80.

652	
653	28. Robinson MD, Oshlack A. 2010. A scaling normalization method for differential expression analysis of RNA-
654	seq data. Genome Biol. 2010;11(3):R25.
655	
656	29. Livak KJ, Schmittgen TD. Analysis of relative gene expression data using real-time quantitative PCR and the
657	2(-Delta Delta C(T)) Method. Methods. 2001;25(4):402-8.
658	
659	30. Miyoshi H, Stappenbeck TS. In vitro expansion and genetic modification of gastrointestinal stem cells in
660	spheroid culture. Nat Protoc. 2013;8(12):2471-82.
661	
662	31. Yan KS, Chia LA, Li X, Ootani A, Su J, Lee JY, et al. The intestinal stem cell markers Bmi1 and Lgr5 identify
663	two functionally distinct populations. Proc Natl Acad Sci U S A. 2012;109(2):466-71.
664	
665	32. Peterson LW, Artis D. Intestinal epithelial cells: regulators of barrier function and immune homeostasis. Nat
666	Rev Immunol. 2014;14(3):141-53.
667	
668	33. Yin X, Farin HF, van Es JH, Clevers H, Langer R, Karp JM. Niche-independent high-purity cultures of Lgr5+
669	intestinal stem cells and their progeny. Nat Methods. 2014;11(1):106-12.
670	
671	34. Park KW, Yang H, Wi H, Ock SA, Lee P, Hwang I-S, et al. Effect of Wnt signaling pathway activation on the
672	efficient generation of bovine intestinal organoids. Journal of Animal Reproduction and Biotechnology.
673	2022;37(2):136-43.
674	
675	35. Clevers H. Modeling Development and Disease with Organoids. Cell. 2016;165(7):1586-97.
676	
677	36. Zietek T, Rath E, Haller D, Daniel H. Intestinal organoids for assessing nutrient transport, sensing and incretin
678	secretion. Sci Rep. 2015;5:16831.
679	
680	37. Gracz AD, Puthoff BJ, Magness ST. Identification, isolation, and culture of intestinal epithelial stem cells

681	from murine intestine. Methods Mol Biol. 2012;879:89-107.
682	
683	38. Gehart H, Clevers H. Tales from the crypt: new insights into intestinal stem cells. Nat Rev Gastroenterol
684	Hepatol. 2019;16(1):19-34.
685	
686	39. Pierzchalska M, Grabacka M, Michalik M, Zyla K, Pierzchalski P. Prostaglandin E2 supports growth of
687	chicken embryo intestinal organoids in Matrigel matrix. Biotechniques. 2012;52(5):307-15.
688	
689	40. Powell RH, Behnke MS. WRN conditioned media is sufficient for in vitro propagation of intestinal organoids
690	from large farm and small companion animals. Biol Open. 2017;6(5):698-705.
691	
692	41. Joo SS, Gu BH, Park YJ, Rim CY, Kim MJ, Kim SH, et al. Porcine Intestinal Apical-Out Organoid Model for
693	Gut Function Study. Animals (Basel). 2022;12(3).
694	
695	42. Lee MG, Lee BR, Lee P, Choi S, Kim J-H, Oh M-H, et al. Apical-out intestinal organoids as an alternative
696	model for evaluating deoxynivalenol toxicity and Lactobacillus detoxification in bovine. Scientific Reports.
697	2024;14(1):31373.
698	
699	43. Derricott H, Luu L, Fong WY, Hartley CS, Johnston LJ, Armstrong SD, et al. Developing a 3D intestinal
700	epithelium model for livestock species. Cell Tissue Res. 2019;375(2):409-24.
701	
702	44. Chandra L, Borcherding DC, Kingsbury D, Atherly T, Ambrosini YM, Bourgois-Mochel A, et al. Derivation
703	of adult canine intestinal organoids for translational research in gastroenterology. BMC Biol. 2019;17(1):33.
704	
705	45. Stewart AS, Freund JM, Gonzalez LM. Advanced three-dimensional culture of equine intestinal epithelial
706	stem cells. Equine Vet J. 2018;50(2):241-8.
707	
708	46. Kawasaki M, Goyama T, Tachibana Y, Nagao I, Ambrosini YM. Farm and Companion Animal Organoid
709	Models in Translational Research: A Powerful Tool to Bridge the Gan Between Mice and Humans, Front Med

710 Technol. 2022;4:895379.

47. Hoffmann P, Schnepel N, Langeheine M, Kunnemann K, Grassl GA, Brehm R, et al. Intestinal organoid-based
 2D monolayers mimic physiological and pathophysiological properties of the pig intestine. PLoS One.
 2021;16(8):e0256143.

48. VanDussen KL, Marinshaw JM, Shaikh N, Miyoshi H, Moon C, Tarr PI, et al. Development of an enhanced human gastrointestinal epithelial culture system to facilitate patient-based assays. Gut. 2015;64(6):911-20.



**Table 1.** Antibodies used to characterise porcine intestinal organoids in this study.

No.	Company (Catalog No.)	Antibody	Host species	Dilution
1	Origene Technologies, Inc. (TA503316)	LGR5	Mouse	1:100
2	Abcam (AB84632)	Cytokeratin 19	Rabbit	1:100
3	Santan Cruz Biotechnology, Inc. (SC-515032)	Mucin2	Rabbit	1:200
4	Abcam (AB38295)	Bmi1	Mouse	1:100
5	BD Biosciences (61081)	E-cadherin	Rabbit	1:100
6	Abcam (AB83746)	F-actin	Mouse	1:200
7	Cell Signaling Technology (9123)	Ki67	Rabbit	1:200
8	Novus Biologicals (NBP1-69466)	Glut2	Rabbit	1:200
9	Biosis (BS-0689R)	PEPT1	Rabbit	1:200

Table 2. Details of the primers used to analyse gene expression in porcine intestinal organoids in this study.

No.	Gene Name	Accession number	Forward	Reverse	Product size(bp)
1	GAPDH	NM_001206359.1	GTCGGTTGTGGATCTGACCT	AGCTTGACGAAGTGGTCGTT	210
2	LGR5	NM_001315762.1	AATTCCCTTTGCTTCCTGGT	GGGCTGATGAATGTGAGGTT	197
3	HNF4A	NM_001044571.1	AGAAATGAACCGGGTGTCTG	GCGGTCGTTGATGTAATCCT	202
4	CDH1	NM_001163060.1	CATCTTCAACCCAACCTCGT	ACGCCTTCATTGGTTACTGG	186
5	GATA6	NM_001044571.1	CTGTCCCCATGACTCCAACT	ATGTACAGCCCGTCTTGACC	178
6	MUC2	XM_021082584.1	AACTGCGAGCAATGTGTCTG	CAGGTCTGCTTGTCTGTGGA	224
7	CHGA	NM_001164005.2	TCGAGGTCATCTCTGACACG	TTCTTCTGCTGATGGGACCT	178